EPR study of orientational and chemical orders in $Rb_x(NH_4)_{1-x}AlF_4$ mixed crystals

1989 J. Phys.: Condens. Matter 1 4585

(http://iopscience.iop.org/0953-8984/1/28/008)

J. Phys.: Condens. Matter 1 (1989) 4585–4598. Printed in the UK

EPR study of orientational and chemical orders in $Rb_x(NH_4)_{1-x}AlF_4$ mixed crystals

A Jouanneaux†‡, A Leblé†, J C Fayet† and J L Fourquet§

† Laboratoire de Spectroscopie du Solide, CNRS UA no 807, Faculté des Sciences, Université du Maine, 72017 Le Mans Cédex, France

§ Laboratoire des Fluorures, CNRS UA no 449, Faculté des Sciences, Université du Maine, 72017 Le Mans Cédex, France.

Received 1 November 1988

Abstract. We show the efficiency of local measurements with an EPR probe by considering the mixed crystals $Rb_x(NH_4)_{1-x}AlF_4$ and the Fe^{3+} probe substituted for Al^{3+}. In pure NH_4AlF_4 we study the orientational order–disorder transition which occurs near 155 K. EPR lineshapes are interpreted from a Kubo–Anderson dynamic model involving random jumps between local configurations, and evidence a crossover 2D–3D in the vicinity of 160 K. In mixed crystals, the room temperature EPR spectra show a random distribution of rubidium and ammonium ions for any x, and allow a simple and accurate measurement of x. At low temperature, we study the influence of the rubidium concentration on the ordering of the ammonium sublattice for $0 < x < 0.25$. For $x > 0.03$, new low temperature orders appear which are interpreted as being structural spin glass phases.

1. Introduction

Previous EPR investigations on $NH_4AlF_4:Fe^{3+}$ evidenced an order–disorder phase transition in the vicinity of $T_c = 155$ K, associated with a full ordering of the ammonium sublattice below 145 K (Leblé *et al* 1982a, b). The structure consists of (001) layers of corner-sharing $[AlF_6]$ octahedra separated by layers of NH_4^+ ions. In both high and low temperature phases, the fluorine octahedra exhibit tilts around the c axis with 'antiferro'-rotational order along c.

At room temperature (RT), the space group is I4/mcm (Fourquet *et al* 1979, Leblé *et al* 1982b) (figure 1) and the NH_4^+ tetrahedra undergo fast reorientations between two equilibrium positions which can be represented by a pseudo-Ising spin operator.

At low temperature (LT), the ammonium ions exhibit a parallel order in the (001) layers and an antiparallel order along the c axis (figures 2(a), (b)). The space group $P4_2/mbc$ was initially inferred from EPR measurements (Leblé *et al* 1982a, b) and confirmed by neutron powder profile refinement (Bulou *et al* 1982).

Recently the dynamics of the phase transition of NH_4AlF_4 has been studied through an EPR investigation on single crystals with the help of a Fe^{3+} probe (Dagorn *et al* 1985). The EPR lineshapes in the temperature range 300 K–145 K have been interpreted quantitatively from a Kubo–Anderson dynamic model involving random jumps between

‡Present address: Laboratoire de Chimie des Solides, CNRS UA No 279, Université de Nantes, 2 rue de la Houssinière, 44072 Nantes Cédex 03, France

0953-8984/89/284585 + 14 $02.50

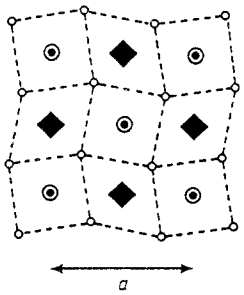

Figure 1. RT structure of NH_4AlF_4. Space group I4/mcm. Projection on (001) of part of the structure bounded by $z = \pm 0.25$. ●: Al at $z = 0$; ○: F_{ax} at $z = \pm 0.14$; ○: F_{eq} at $z = 0$; ◆: NH_4 at $z = \pm 0.25$.

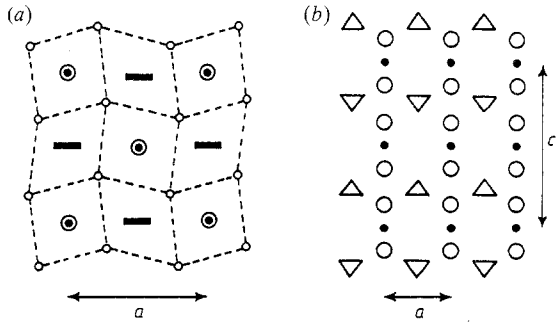

Figure 2. LT structure of NH_4AlF_4. Space group $P4_2/mbc$: (*a*) Projection on (001) of part of the structure bounded by $z = \pm 0.25$. Symbols as in figure 1 and ▬: H–H edge at $z = +0.20$. (*b*) Section parallel to (010) at $y = 0$. Symbols as in figure 1 and △, ▽: two possible orientations of the NH_4^+ ions.

local configurations, and have shown the existence of a crossover 2D–3D in the vicinity of 165 K.

In this paper, we present a refinement of the model used in the above-mentioned paper. Our refined model enables, in particular, the effective dimensionality of the lattice versus the temperature to be followed accurately. We also report an EPR investigation in the disordered system $Rb_x(NH_4)_{1-x}AlF_4$ using the Fe^{3+} probe. $RbAlF_4$ exhibits almost the same atomic structure as NH_4AlF_4, except for the rotational order of the fluorine octahedra along ***c***, which is of ferro-type (space group P4/m***b***m) (Bulou and Nouet 1982). The first EPR experimental results concerning these mixed crystals are briefly reported elsewhere (Jouanneaux *et al* 1987). Our main purpose is to show the efficiency of local measurements with the Fe^{3+} probe substituted for Al^{3+} ions, to characterise an orientational order–disorder transition, and to point out some basic mechanisms responsible for the confused lineshapes which are normally observed in disordered systems.

2. Experimental

Single crystals of $Rb_x(NH_4)_{1-x}AlF_4$ were grown by means of hydrothermal synthesis. Small amounts of Fe_2O_3 were added in the starting mixture. (This was done by one of us (JLF)).

The EPR spectra were recorded on a Bruker X-band spectrometer ($\nu \simeq 9.5$ GHz). The static magnetic field may be varied from 0 to 10000 G. In the range 300–100 K, we have used the standard Bruker variable-temperature system where the temperature at the sample is established by regulating the temperature of N_2 gas streaming past the sample. At lower temperature, the spectrometer was equipped with a helium gas-flow cryostat (Oxford Instruments). The temperature stability was better than 0.1 K.

The simulation of the EPR spectra of pure NH_4AlF_4 with the dynamic model was performed with a program written by one of us (AL). The simulation of the EPR spectra of mixed crystals has been achieved with a general program which adds single lines of given position, intensity, width and shape and which works in interactive mode on a microcomputer.

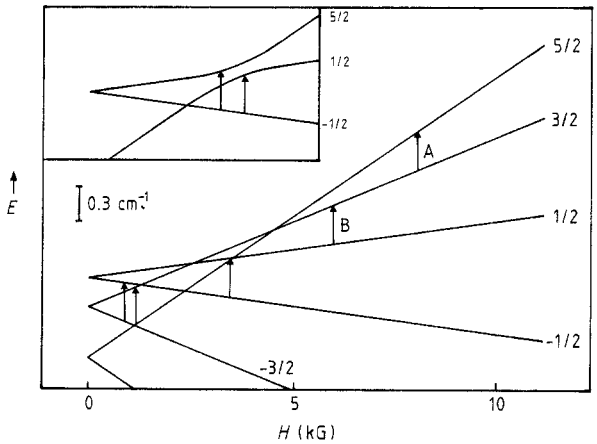

Figure 3. Energy levels and EPR transitions in $NH_4AlF_4:Fe^{3+}$ at RT for $\boldsymbol{H} \parallel \boldsymbol{c}$. Inset: influence of a spin-level decrossing (from Leblé *et al* 1982a, b).

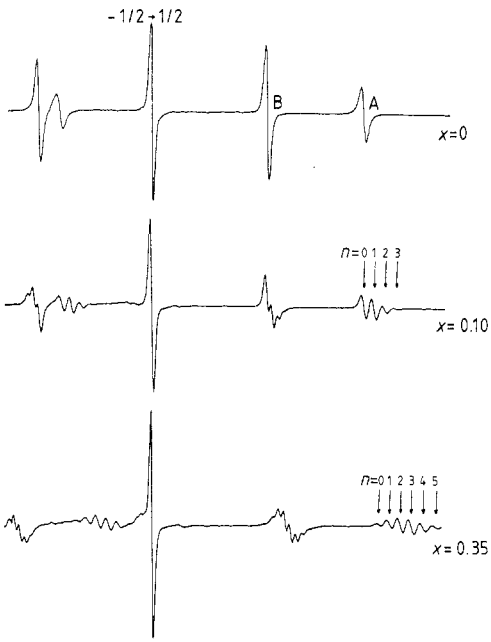

Figure 4. Examples of RT spectra of $Rb_x(NH_4)_{1-x}AlF_4:Fe^{3+}$ for $\boldsymbol{H} \parallel \boldsymbol{c}$. H varies from 0 to 10000 G.

3. Local order in $Rb_x(NH_4)_{1-x}AlF_4$ at room temperature

3.1. EPR spectra for $Rb_x(NH_4)_{1-x}AlF_4:Fe^{3+} - \boldsymbol{H} \parallel \boldsymbol{c}$

Figure 3 depicts the energy levels and EPR transitions of the Fe^{3+} probe for pure NH_4AlF_4 when $\boldsymbol{H} \parallel \boldsymbol{c} \equiv [001]$. For this orientation of the magnetic field, the energy levels are linear and the EPR spectrum shows the classical five transitions $M_s \rightarrow M_s + 1$. The positions of the A and B lines (figures 3 and 4) depend only on the value of the axial quadrupolar parameter $b_2^0 = -1112 \times 10^{-4}\ cm^{-1}$, which reflects the average quadratic symmetry at the Al^{3+} site (Leblé *et al* 1982b).

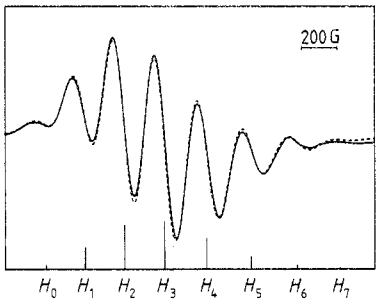

Figure 5. Simulation of the $\{A\}$ transition for $x = 0.35$ at $T = 300$ K: ——; experimental spectrum – – –; calculated spectrum according to random substitution. H_n represent the line positions for the second shell $[Rb_n(NH_4)_{8-n}]$.

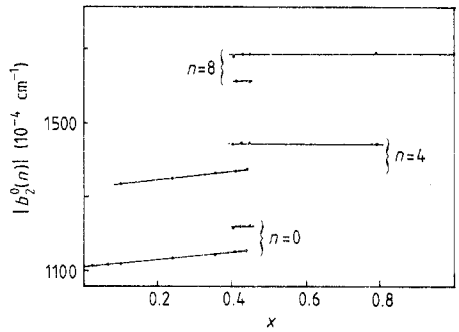

Figure 6. Dependence on x of the axial parameter $b_2^0(n)$ for a configuration $[Rb_n(NH_4)_{8-n}]$ at RT for $n = 0, 4, 8$.

In mixed crystals $Rb_x(NH_4)_{1-x}AlF_4$ ($x \neq 0$) for $\boldsymbol{H} \| \boldsymbol{c}$, each transition (except the $-\frac{1}{2} \rightarrow \frac{1}{2}$ transition) exhibits a well resolved structure (figure 4) that represents the distribution of local crystal fields. The lines of the structures, labelled by n, are attributed to Fe^{3+} probes surrounded, as next-nearest neighbours, by n Rb^+ ions and $(8-n)$ NH_4^+ ions.

For any concentration x, the A (and B) transitions may be perfectly reconstructed (figure 5) according to

$$F(H,x) = \sum_{n=0}^{8} I_n(x) f[(H - H_n(x))/L(x)]$$

with $I_n(x) = C_8^n x^n (1-x)^{8-n}$ by fitting x, the lineshape f, the linewidth $L(x)$ and the position of the centre of the line $H_n(x)$.

The formula used for the relative intensity $I_n(x)$ corresponds to a random distribution of the Rb^+ and NH_4^+ ions. Then the simulation of the EPR lines indicates that no chemical ordering occurs in mixed crystals for any x, and provides us with a very simple and rapid means of measuring the rubidium concentration with a good accuracy ($\Delta x/x \simeq 3\%$). It shows equally the short range character of the Fe^{3+} probe, because the position of the lines is essentially influenced by the configuration of the 8-shell of monovalent neighbours.

3.2. Evolution of $b_2^0(n)$ versus the concentration

In figure 6, we have plotted the values of the local crystal field parameter $b_2^0(n)$, measured from the positions of the A and B lines, versus the chemical composition x. n represents the number of Rb^+ ions substituted for NH_4^+ in the 8 second-shell.

For $x < 0.40$, $|b_2^0(n)|$ increases linearly versus the concentration, starting from the value of pure NH_4AlF_4 for $n = 0$. For $x > 0.45$, $b_2^0(n)$ does not depend significantly on x, and has practically the value of pure $RbAlF_4$ for $n = 8$.

Considering that, at RT, the main difference between the structures of pure $RbAlF_4$ and NH_4AlF_4 concerns the ordering of the fluorine octahedra along c, these results tend to suggest that the average structures of mixed crystals are of NH_4AlF_4 type for $x < 0.40$

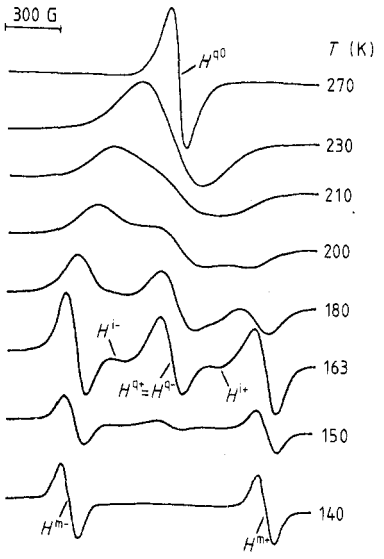

Figure 7. EPR spectra of $NH_4AlF_4:Fe^{3+}$ from 300 K to 140 K for $\boldsymbol{H} \parallel [100]$.

(space group I4/mcm) and of $RbAlF_4$ type for $x > 0.45$ (space group P4/mbm). Eventually, for $0.40 < x < 0.45$ and for different samples, two values of $b_2^0(n)$ are observed, probably corresponding to two possible types of crystal structure, depending on the exact conditions (P, T) of the hydrothermal growth. X-ray measurements will be made to confirm this simple hypothesis.

4. EPR study of the phase transition of pure NH_4AlF_4: refinement of the dynamic model

4.1. Introduction

The temperature dependence of the high-field line (called the E line) in $NH_4AlF_4:Fe^{3+}$ for $\boldsymbol{H} \parallel [100]$ is represented in figure 7. The experimental work on which this figure is based is reported elsewhere (Leblé *et al* 1982a, b).

At RT, the average quadratic symmetry at the Al^{3+} site gives a single line. On cooling, the lineshapes clearly exhibit motional effects: slowing down; precursor order clusters represented by a lateral doublet below 210 K; and a full LT order below 150 K marked by a splitting of the RT line. This splitting results from a lowering of the Al^{3+} point symmetry from 4/m to 2/m and corresponds to an asymmetry of the local crystal field characterised by the spin-Hamiltonian parameter $|b_2^2| = 280 \times 10^{-4}\,cm^{-1}$. In other words, the LT doublet is associated with equivalent sites with asymmetry axes denoted by $\pi/2$ around the c axis.

Only a parallel ordering of the NH_4^+ tetrahedra in the (001) layers and an antiparallel ordering along the c axis lead to a 2/m symmetry at the Al^{3+} site (figure 2(b)) (Leblé *et al* 1982a, b). Any different ordering would lead to a 4/m or $\bar{4}$ local symmetry. Thus, the LT space group $P4_2/mbc$ was immediately deduced from the EPR spectra and this result has been confirmed later by neutron powder diffraction (Bulou *et al* 1982).

Then, using the Kubo–Anderson theory of motional narrowing (Kubo 1954, Anderson 1954, Abragam 1961), a dynamic model involving a relaxation process between five local atomic configurations was set up to interpret the EPR lineshapes in the temperature

Table 1. Magnetic field line positions associated to the possible values of the pseudo-spin $\Sigma = \sigma_1 - \sigma_2$. σ_1 and σ_2 represent the local order of the NH_4^+ ions located above and below the Fe^{3+} probe. $\sigma = \pm 1$: order. $\sigma = 0$: disorder.

σ_1	−1	−1 0	−1	0	1	0 1	1
σ_2	1	0 1	−1	0	1	−1 0	−1
Σ	−2	−1 −1	0	0	0	−1 −1	2
b_2^2 (10^{-4} cm^{-1})	−280	−140	0	0	0	140	280
Line positions	H^{m-}	H^{i-}	H^{q-}	H^{q0}	H^{q+}	H^{i+}	H^{m+}

range 300–145 K (Dagorn *et al* 1985). The results of calculations revealed a steep increase of the occupation probability of the LT-ordered configurations between 160 K and 150 K. Then a simple 'geometrical' model was set up in order to connect the dimensionality of the correlations with the variations of the occupation probabilities versus the temperature directly. It was finally found that a dynamic crossover 2D–3D occurred in the vicinity of 165 K.

In this section, we present a refinement of the initial model, with the following improvements:

(i) We have used a pseudo-spin of block representation to determine the different local configurations. Then we obtain a more realistic relaxation scheme involving nine local configurations instead of five. This enables us to dissociate the temperature behaviour of the quadratic configurations corresponding to a full local disorder and to a ferro-local order. Indeed, the occupation probability of the latter is essential to characterise the 3D ordering (§ 4.2).

(ii) We have used the 'geometrical' model directly in order to follow the temperature dependence of the dimensionality of the correlations between ammonium ions (§ 4.3).

4.2. Pseudo-spin representation—local configurations

Consistent with the short range of the probe, experimentally demonstrated by the line structure in mixed crystals, the local configurations of the NN NH_4^+ tetrahedra can be grouped into key configurations, analysing the microscopic mechanisms involved in the parameter b_2^2.

Let us first consider one Fe^{3+} ion located between two NH_4^+ adjacent layers and let us use a pseudo-spin σ to describe the local order of the NH_4^+ ions. We take $\sigma = 0$ for the disorder, and $\sigma = \pm 1$ for the two possibilities of parallel order in a layer. Let us now consider the block of eight ammonium ions surrounding an Fe^{3+} probe substituted for an Al^{3+} ion. The local order of the configuration is characterised by the pseudo-spin $\Sigma = \sigma_1 - \sigma_2$, where σ_1 and σ_2 are the pseudo-spins of four NH_4^+ ions above and below the Fe^{3+} probe respectively.

The possible values of Σ are $-2, -1, 0, 1, 2$ (table 1), for which are associated the following key configurations.

(i) $\Sigma = \pm 2$ corresponds to the LT-ordered configurations (precursor-order cluster). The local crystal field parameter is $b_2^2 = b_2^2\ (T < T_c) = \pm 280 \times 10^{-4}$ cm^{-1}.

(ii) $\Sigma = \pm 1$ corresponds to the intermediate order: local order exists in one layer, but disorder occurs between the adjacent layers. For such configurations, only one half of the NH_4^+ ions cooperate to the local crystal field asymmetry and $b_2^2 = \frac{1}{2}b_2^2\ (T < T_c) = \pm 140 \times 10^{-4}$ cm^{-1}.

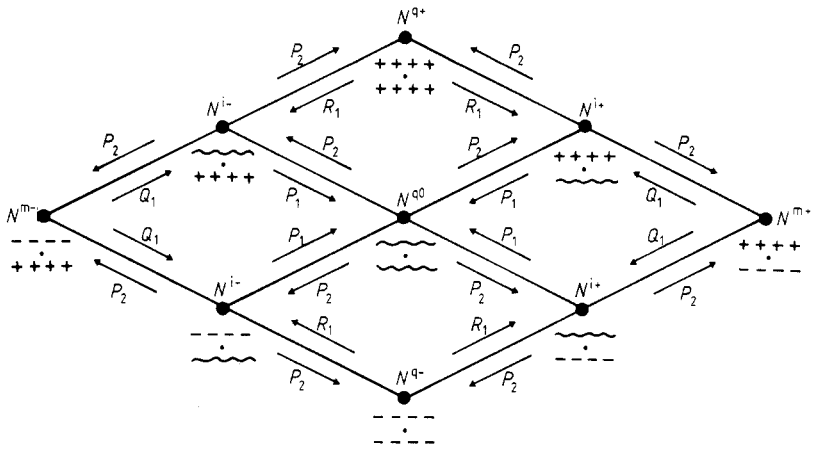

Figure 8. Relaxation scheme: local configurations of the ammonium ions close to the Fe^{3+} probe. ++++: 2D parallel order with up orientation of the NH_4^+ ions ($\sigma = +1$) in a (001) layer. ----: 2D parallel order with down orientation ($\sigma = -1$). ~~~~ : 2D disorder ($\sigma = 0$). ●: $Al^{3+}(Fe^{3+})$. $N^{\alpha\beta}$ (with α = m, i, q and $\beta = +, 0, -$) represent the occupation probabilities. P_1, P_2, Q_1, R_1: jump probabilities.

(iii) $\Sigma = 0$ with $\sigma_1 = \sigma_2 = \pm 1$ corresponds to a local parallel order of the NH_4^+ ions in adjacent layers and ferro-order between them. The local symmetry at the Al^{3+} site is $\bar{4}$ and $b_2^2 = 0$.

(iv) $\Sigma = 0$ with $\sigma_1 = \sigma_2 = 0$ corresponds to the full disorder, restoring an average quadratic symmetry, and $b_2^2 = 0$.

The qualitative relevance of this classification, based on an underlying superposition model, is apparent on the EPR spectra (figure 7): the configurations (i) are responsible for the lateral doublet (H^{m-}, H^{m+}). The configurations (ii) correspond to an intermediate doublet (H^{i-}, H^{i+}), which is necessary to explain the lineshape in the slow regime below 180 K. The configurations (iii) and (iv) are responsible for the central lines ($H^{q+} = H^{q-} \simeq H^{q0}$). The main interest of this classification is to dissociate the behaviour of these two configurations, which contribute to the same line position.

As for the initial model, we have used a Kubo–Anderson dynamic model involving a relaxation process between the nine possible local configurations, random jumps with many reorientations of the NH_4^+ ions being forbidden. The relaxation scheme is represented in figure 8, where we have used a pseudo-spin (+, −) representation for the two possible orientations of the NH_4^+ tetrahedra. The symmetry implies $N^{\alpha+} = N^{\alpha}$ with α = m, i, q and also leads to a limited number of independent jump probabilities.

4.3. *'Geometrical' model*

The ultimate improvement of our model has been the direct use of a 'geometrical' model which enables the dimensionality of the correlations to be connected with the variations of the occupation probabilities versus the temperature.

Let us represent by s the density of 2D parallel ordered clusters ($\sigma = \pm 1$) in one (001) ammonium layer. Then $1 - s$ is the relative area of disordered regions ($\sigma = 0$). The minimum value of s is $s_{min} = \frac{1}{8}$, which corresponds to the probability to obtain $\sigma = \pm 1$, if the four ammonium ions of a block are situated randomly. Let us also consider an

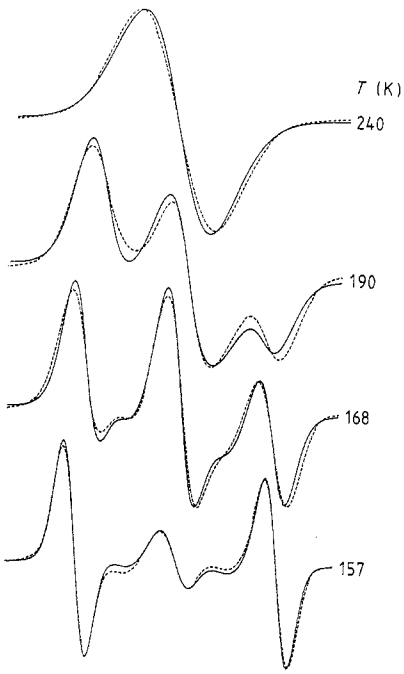

Figure 9. Computer reconstruction of the E lines at $T = 157$, 168, 190 and 240 K with the Kubo–Anderson model. ——: experimental and – – – calculated spectra.

additional coupling parameter v between the NH_4^+ layers that favours the low-temperature 3D order. Then the occupation probabilities can be easily expressed as a function of s and v according to:

$$P(\mathrm{i}) = N^{\mathrm{m}+} + N^{\mathrm{m}-} = \tfrac{1}{2}s^2(1+v) \qquad P(\mathrm{ii}) = 2(N^{\mathrm{i}+} + N^{\mathrm{i}-}) = 2s(1-s)$$

$$P(\mathrm{iii}) = N^{\mathrm{q}+} + N^{\mathrm{q}-} = \tfrac{1}{2}s^2(1-v) \qquad P(\mathrm{iv}) = N^{\mathrm{q}0} = (1-s)^2$$

and they verify the condition: $P(\mathrm{i}) + P(\mathrm{ii}) + P(\mathrm{iii}) + P(\mathrm{iv}) = 1$.

Moreover, the jump probabilities, being connected to the occupation probabilities through the balance equation, can be written as a function of P_1, s, v:

$$P_2 = P_1 s/2(1-s) \qquad Q_1 = P_1/(1+v) \qquad R_1 = P_1/(1-v).$$

Then the lineshape can be calculated from this model, by fitting P_1, s, v and the magnetic field line positions associated with the different configurations. We will not discuss here the application of the Kubo–Anderson theory to EPR experiments. This has been clearly explained in the paper of Dagorn *et al* (1985).

For the simulation of the EPR spectra, we have used a continuous process from 145 to 300 K with temperature jumps of a few degrees. Some characteristic computer reconstructions of the experimental line are represented in figure 9.

4.4. Results of calculations

The results of the fit are shown in figures 10, 11, 12, which depict the temperature dependence of s and v, of the occupation probabilities $P(\mathrm{i})$, $P(\mathrm{ii})$, $P(\mathrm{iii})$, $P(\mathrm{iv})$ and of the inverse lifetime $\tau^{-1} = Q_1$ of precursor order clusters.

At 300 K, s reaches the value of 0.15 (figure 10), which is not far from the minimum value $s_{\min} = \frac{1}{8}$ corresponding to the absence of correlation between the ammonium ions.

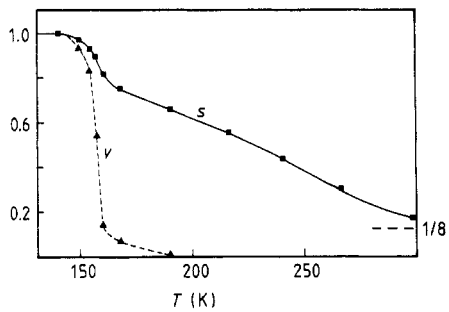

Figure 10. Dependence on temperature of the parameters s and v.

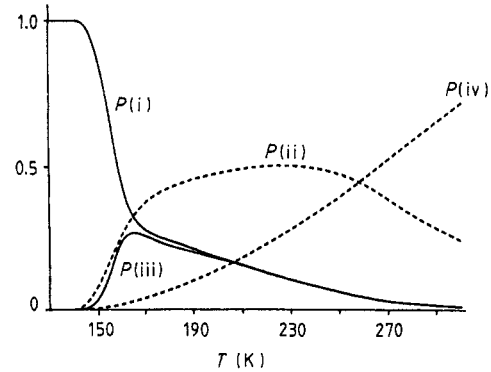

Figure 11. Occupation probabilities of the different key configurations.

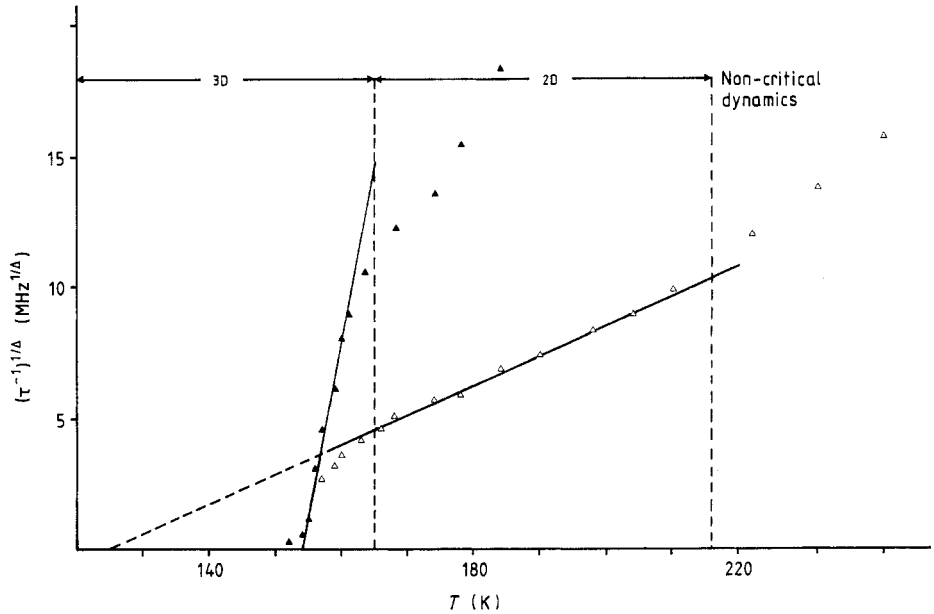

Figure 12. Exponent laws for the inverse lifetime τ^{-1} of precursor order clusters. ▲ : Δ = 1.30; △ : Δ = 2.

This result confirms our hypothesis about the pseudo-spin σ associated with a square of four ammonium ions.

From 300 K down to 170 K, it is found that P(i) = P(iii) (figure 11). This means that in this temperature range the ordering process is essentially bidimensional: parallel or antiparallel orders along c are equivalent. It can be also noted that $P(\text{ii})_{\max} = \frac{1}{2}$ in a 2D regime, and this is experimentally verified.

At lower temperature, the rise of the 3D ordering of the ammonium sublattice is marked by the fast decrease of P(iii) and by the sharp increase of the density of 3D-ordered clusters P(i), which are concomitant with the sharp increase of the coupling parameter v between 160 K and 150 K. In this temperature range, s is not too far from the value $s = 1$. Then we conclude that the crossover 2D–3D occurs in the vicinity of 160 K.

According to figure 12, three different regimes can be observed for the inverse lifetime τ^{-1} of precursor-ordered clusters. In the temperature range 165–215 K, τ^{-1} verifies an exponent law $\tau^{-1} \propto (T - T_c(2D))^{\Delta}$ with $T_c(2D) = 125$ K and $\Delta = 2$, this exponent being characteristic of the critical slowing-down for a 2D Ising system. At lower temperature, τ^{-1} deviates downwards from the 2D regime and obeys the exponent law $\tau^{-1} \propto (T - T_c(3D))^{\Delta}$ with $T_c(3D) = 154$ K and $\Delta \simeq 1.30$, the critical index for a 3D Ising system. $T_c(3D) = 154$ K belongs to the steep-rise region observed for $P(i)$ and v. Thus the crossover 2D–3D is also apparent in the critical slowing-down which may be characterised by critical exponents function of the critical exponent ν for the correlation length of 2D and 3D Ising systems.

Above 215 K, τ^{-1} deviates upwards from the 2D regime, and verifies an Arrhenius law with an activation energy $E = 1630$ K, which is in good agreement with NMR results (Bulou 1983). Then the NH_4^+ tetrahedra reorient independently of their surrounding in a local double-well potential, where E is the depth of the wells.

Finally, it must be stressed that near $T_c(3D)$, the almost static EPR spectrum exhibits essentially an LT doublet and a central quadratic line on a flat absorption background. This is characteristic of very large 2D domains with a parallel order in the (001) ammonium layers ($s > 0.9$), and the quadratic line can be assigned to flat antiphase walls in the LT 3D ordering of the ammonium sublattice.

5. LT ammonium ordering in $Rb_x(NH_4)_{1-x}AlF_4$ mixed crystals

5.1. Experimental results—simulation of the {E} lines

The LT $\{E\}$ lines for $\boldsymbol{H} \parallel [100]$ are represented in figures 13(a) and 13(b) for $x = 0.043$ and $x = 0.067$ respectively. The rubidium concentration of these mixed crystals was measured at RT from the simulation of the $\{A\}$ lines for $\boldsymbol{H} \parallel \boldsymbol{c}$.

Qualitatively, up to $x = 0.10$, the essential features of the critical slowing-down are modified little with respect to pure NH_4AlF_4 (figure 7), but the $\{E\}$ lines associated with $n = 0$ are flanked by satellites due to NN Rb^+ ions substituted for NH_4^+ ions, and become really messy for $x > 0.10$. Moreover, the LT static spectra relative to mixed crystals (figure 13) are quite different from the one obtained in pure NH_4AlF_4, but mirror stable phases with frozen orientations of the ammonium ions.

The lineshapes up to $x = 0.10$ can be accurately reconstructed by a well defined monoclinic doublet (m_1, m_2) as in the LT phase of pure NH_4AlF_4 and by a central quadratic line q (figure 13). These lines correspond to a second shell of eight ammonium ions ($n = 0$). The other lines observed on figure 13 are associated with configurations with $n = 1$ or $n = 2$ rubidium ions randomly substituted for NH_4^+ ions.

The relative number of quadratic sites N_q is deduced from the simulation of the $\{E\}$ lines and is proportional to the total intensity of the 'quadratic' lines associated with $n = 0, 1 \ldots$. It may be stressed that the relative intensity of the q line rapidly increases between $x = 0.043$ and $x = 0.067$ (figure 13). The results of these measurements are given in table 2. For $x = 0.24$, the value of N_q was not measured from the simulation of the LT $\{E\}$ lines, which becomes barely tractable for $x > 0.10$. We have used another magnetic field orientation (§ 5.2.).

On the other hand, the computer reconstruction of the EPR spectra indicates that the Rb^+ ions perturb the monoclinic and quadratic lines randomly. Thus the quadratic sites

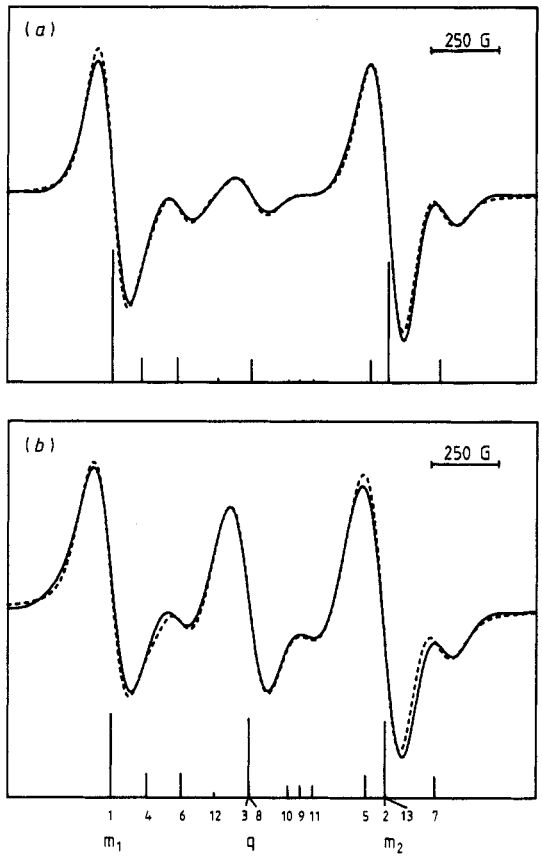

Figure 13. $\{E\}$ lines for $\boldsymbol{H} \parallel [100]$ at $T = 100$ K for $x = 0.043$ (a); $x = 0.067$ (b). ——: experimental spectra. – – – –: simulated spectra with 13 single lines. $(1, 2) \equiv (m_1, m_2)$: monoclinic doublet ($n = 0$); $3 \equiv q$: quadratic line ($n = 0$); (4, 5), (6, 7): monoclinic doublets ($n = 1$); (8, 9), (10, 11): pseudo-quadratic doublets ($n = 1$); (12, 13): the more intense monoclinic doublet ($n = 2$).

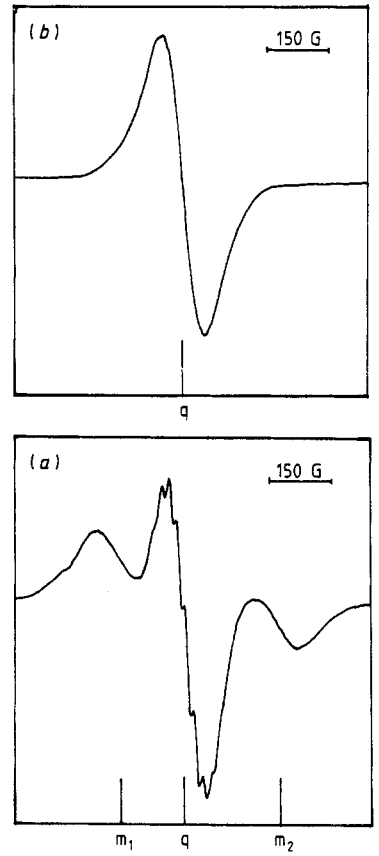

Figure 14. Experimental EPR lines for $\boldsymbol{H} \parallel [001]$ at $T = 100$ K for $x = 0.067(a)$ and $x = 0.24(b)$. (m_1, m_2): monoclinic doublet; q: quadratic line.

Table 2. Relative number of 'quadratic' sites N_q for different Rb^+ concentrations.

x	0.008	0.028	0.043	0.067	0.10	0.24
N_q	$\sim 10^{-2}$	$\sim 10^{-2}$	0.075(5)	0.33(2)	0.48(5)	>0.90

are not preferentially pinned by the rubidium ions. However, no diffuse absorption background corresponding to local disorder is apparent.

5.2. *Estimation of N_q for $x = 0.24$*

For $x > 0.10$, the LT $\{E\}$ lines for $\boldsymbol{H} \parallel [100]$ become really confused, because of the many overlapping lines arising from local configurations with $n = 0, 1, 2, 3$ or more Rb^+ ions. In order to determine N_q for $x = 0.24$, we have studied the EPR spectra for $\boldsymbol{H} \parallel [001]$.

In pure NH_4AlF_4, the transition $-\frac{1}{2} \rightarrow \frac{1}{2}$ at RT for $\boldsymbol{H} \parallel [001]$ occurs near a level crossing involving $M_s = \frac{1}{2}$ and $M_s = \frac{5}{2}$ (figure 3). At LT, the asymmetry of the local crystal field represented by the parameter b_2^2 can split this single line into a monoclinic doublet through a level decrossing, mixing $M_s = \frac{1}{2}$ and $M_s = \frac{5}{2}$ (see inset in figure 3).

The evolution of the LT phase in mixed crystals can be followed through this transition. In the range $x = 0.043$ to $x = 0.10$, the LT EPR spectrum evidences a monoclinic doublet (m_1, m_2) due to sites with a substantial crystal field asymmetry, as for the LT phase of pure NH_4AlF_4, and a central quadratic line q (figure 14(*a*)). This quadratic line exhibits a well resolved SHF ^{19}F structure, not resolved at RT. This is the mark of a well defined static local order. Moreover, for this orientation of the magnetic field, the perturbations by the rubidium ions are not resolved.

For $x = 0.24$, one observes only a quadratic line, with no evidence of sites with a substantial crystal field asymmetry. The SHF structure is not resolved (figure 14(*b*)). because of the line broadening through topological disorder. The value of N_q cannot be measured accurately; nevertheless we may infer from the existence of a single quadratic line that N_q is not too far from the value $N_q = 1$.

5.3. Discussion

All the previous observations are consistent with a rather long-range 2D parallel order of the ammonium ions in the (001) layers. Moreover, the quadratic lines that persist at very low temperature are due to Fe^{3+} probes located between adjacent ammonium layers exhibiting a parallel order along the *c* axis. These adjacent layers with a parallel order may represent antiphase walls.

For $x < x_c$ ($0.028 < x_c < 0.043$) the density of antiphase walls given by N_q is about 1%, and the 3D ordering of the ammonium sublattice settles as for pure NH_4AlF_4, according to recent neutron diffraction results (Jouanneaux *et al* 1989).

For $x > x_c$, the relative number of quadratic sites N_q increases radically with x. This clearly indicates that the ordering of adjacent ammonium layers is no longer fully antiparallel along *c*: a new LT phase occurs. The neutron diffraction measurements have shown that these phases do not correspond to high-order commensurate phases, such as are given by extended Ising models with competing interactions (Selke *et al* 1985, Barreto and Yeomans 1985). Finally, the actual LT phase for $x > x_c$ is similar to a structural pseudo-spin glass phase, with long range 2D-ordered domains exhibiting static disorder along the *c* axis. Eventually, for $x = 0.24$, we may infer, from the value of N_q, that the LT 3D order of the ammonium sublattice tends to become fully parallel.

From these results, it turns out that the phase diagram (x, T) of the $Rb_x(NH_4)_{1-x}AlF_4$ system is rather similar to the one observed for $Rb_{1-x}(NH_4)_xH_2PO_4$ (Courtens 1982, Cowley *et al* 1985) and for magnetic alloys with competing ferro–antiferro interactions (Aharony 1978). Nevertheless, in the system $Rb_x(NH_4)_{1-x}AlF_4$, the static disorder of the NH_4^+ ions in the glassy phase probably does not result from directly competing interactions between the pseudo-spins.

Until now, the LT ordering of the NH_4^+ sublattice was considered independently of the organisation of the fluorine octahedra. In pure NH_4AlF_4, the short range octupole–octupole interaction between the NH_4^+ tetrahedra is not strong enough to explain the LT phase, and we may consider that the antiferro-type rotation of the AlF_6 octahedra favours the LT order of the ammonium sublattice (Leblé *et al* 1982b). Considering that the AlF_6 octahedra are ferro-rotationally ordered in $RbAlF_4$, we may then question the nature of the rotation of fluorine octahedra in mixed crystals, and therefore the influence

of the organisation of the AlF_6 sublattice on the LT orientational ordering of the ammonium ions.

The Fe^{3+} probe is not sufficiently sensitive to measure the local tilts of the octahedra around c, and is not well situated to control the rotational order between adjacent layers of $[AlF_6]$ groups. For this latter purpose, a probe substituted for the monovalent cation should be further adapted. Let us remind ourselves that in $SrTiO_3$ the antiferro distorsive order of the LT phase could be fully demonstrated by using two probes, one substituted for a Ti^{4+} ion, the other one for a Sr^{2+} ion (Unoki and Sakudo 1967, Müller and Berlinger 1971). At present, we cannot exclude the hypothesis that disorder in the organisation of the $[AlF_6]$ sublattice finally drives the LT ordering of the NH_4^+ ions in the glassy phase. This remains an open question.

6. Conclusion

In this paper, we have shown the efficiency of the use of the EPR technique to study various features of a disordered system.

In pure NH_4AlF_4, we have studied the orientational order–disorder transition, and all the essential features (LT static order, depth of the local wells, precursor-order clusters, collective dynamics, effective dimensionality of the lattice) spring from the EPR lines. The Fe^{3+} probe enables the configurations of blocks of pseudo-spin to be monitored through four types of lines. This may evoke the first step of a Kadanoff transformation of the NH_4^+ sublattice.

In mixed crystals, EPR local measurements at room temperature are efficient to verify the random distribution of the rubidium ions, and to measure accurately the concentration for each crystal. The measurement of $b_2^0(n)$ shows a discontinuity of the structure when going from NH_4AlF_4 to $RbAlF_4$. At low temperature, we have been able to determine the local and 2D orders of the ammonium ions, and to observe the influence of the rubidium concentration on the LT ordering of the ammonium sublattice.

X-ray diffraction experiments are now necessary in order to confirm the hypothesis of a discontinuity of the crystallographic structure at room temperature for $0.40 < x < 0.45$. Neutron diffraction measurements will also have to be performed for $x = 0.24$ to verify the possible 3D order of the ammonium sublattice at low temperature.

References

Abragam A 1961 *Les Principes du Magnétisme Nucléaire* (Paris: PUF) p 445–8
Aharony A 1978 *J. Mag. Magn. Mat.* **7** 198
Anderson P W 1954 *J. Phys. Soc. Japan* **9** 316
Barreto M and Yeomans J 1985 *Physica A* **134** 84
Bulou A 1983 private communication
Bulou A, Leble A, Hewat A W and Fourquet J L 1982 *Mater. Res. Bull.* **17** 391
Bulou A and Nouet J 1982 *J. Phys. C: Solid State Phys.* **15** 183
Courtens E 1982 *J. Physique Lett.* **L199** 43
Cowley R A, Ryan T and Courtens E 1985 *J. Phys. C: Solid State Phys.* **18** 2793
Dagorn Y, Leblé A and Fayet J C 1985 *J. Phys. C: Solid State Phys.* **18** 383
Fourquet J L, Plet F, Courbion G, Bulou A and De Pape R 1979 *Rev. Chim. Miner.* **16** 490
Jouanneaux A, Leblé A, Fayet J C and Fourquet J L 1987 *Europhys. Lett.* **3** 61
Jouanneaux A, Leblé A, Pannetier J and Fourquet J L 1989 *J. Phys. Condens. Matter* **1** 1577–88
Kubo R 1954 *J. Phys. Soc. Japan* **9** 935

Leblé A, Rousseau J J, Fayet J C and Jacobini C 1982a *Solid State Commun.* **43** 773
Leblé A, Rousseau J J, Fayet J C, Pannetier J, Fourquet J L and De Pape R, 1982b *Phys. Status Solidi* a **69** 249
Müller K A and Berlinger W 1971 *Phys. Rev. Lett.* **26** 13
Selke W, Barreto M and Yeomans J 1985 *J. Phys. C: Solid State Phys.* **18** L393
Unoki H and Sakudo T 1967 *J. Phys. Soc. Japan* **23** 546